CrossMark

Near-infrared absorbing squaraine dye with extended π conjugation for dye-sensitized solar cells

Claudio Magistris [a,1], Stefano Martiniani [b,1], Nadia Barbero [a], Jinhyung Park [a],
Caterina Benzi [a], Assaf Anderson [b], ChunHung Law [b], Claudia Barolo [a,*], Brian O'Regan [b]

[a] Dipartimento di Chimica, NIS Centre of Excellence, Università di Torino, Via Pietro Giuria 7, I-10125 Torino, Italy
[b] Department of Chemistry, Imperial College London, Imperial College Road, London SW7 2AZ, UK

ABSTRACT

A NIR absorbing squaraine dye has been synthesized as a sensitizer for use in dye-sensitized solar cells (DSCs). Following computational calculations, a benz[cd]indole moiety was selected as an electron-rich heterocyclic component and condensed with indole-based emisquaraine bearing a carboxyl group, as an anchor for their immobilization on TiO_2, to obtain an unsymmetrical squaraine with extended absorption due to its extensive π conjugation. The cells based on this dye exhibited a spectral response in the near-infrared region over 750 nm in addition to the visible region with a light absorption edge at 900 nm. The cells showed 1.1% efficiency and Incident Photon Current Efficiency (IPCE) of 36% at 800 nm.

© 2013 Elsevier Ltd. All rights reserved.

1. Introduction

Dye-sensitized solar cells (DSCs) have attracted considerable attention due to their relatively high solar energy conversion efficiency and low cost [1]. State-of-the-art DSCs are currently characterized by solar-to-electric power conversion efficiencies (PCEs), ranging around 350–750 nm, of 10–13% [2,3]. The main limit is the lack of absorption in the far-red/near-IR region limiting further improvement in efficiency. Therefore, development of new sensitizers with extended absorption into the infrared region is essential [4]. Squaraine [5], phthalocyanine [6], cyanine, porphyrin [7] and croconate dyes [8] are well documented for their intense absorption bands in the near infrared region and have recently received considerable attention because of their possible applications such as solar cells [9,10], photodynamic therapy [11], lasers, and optoelectronic devices [12].

Several groups have used near-IR dyes as sensitizers in DSCs obtaining rather low conversion efficiencies. This is mainly due to the formation of aggregates and the difficulty to obtain dyes with appropriate energy levels of the excited states, that is with a LUMO sufficiently high in energy to allow for fast electron injection and a HOMO sufficiently low in energy to allow for fast regeneration. This is particularly difficult to achieve for near-IR dyes where the $\Delta E_{HOMO-LUMO}$ has to be maintained as small as possible. Therefore, other strategies have to be adopted to guarantee fast injection and fast regeneration in near-IR dye based cells [13]. Another disadvantage of near-IR dyes is their low stability under thermal stress and in the light-soaking test. Therefore, molecular engineering of near-IR dyes with a high photovoltaic performance and an enhanced stability is necessary [14].

So far NIR sensitization was achieved using a panchromatic ruthenium sensitizer based on π-conjugated quaterpyridines [15–17] and terpyridine [18] yielding an IPCE from 360 nm up to 920 nm, with 33% efficiency at 800 nm. Nickel bis(dithiolene) complexes, exhibiting intense absorption bands below 400 nm and broad absorption bands with high molar extinction coefficients in the NIR region (700–1100 nm), were also used as DSCs sensitizers but their energy conversion efficiencies were in the range of 0.07–0.11% [19]. A polymer dye was also employed with an absorption peak maximum at 820 nm and showed a cell efficiency of 1.2% [20]

To date, the best NIR dye reported in literature is a symmetrical cyanine dye with maximum absorption band at around 850 nm [21]. An efficiency as high as 2.3% for the infrared-dye-sensitized solar cell was obtained by adjusting the concentration of deoxycholic acid (DCA) in the dye solution but working with a considerably thick (22–26 μm) TiO_2 electrode with a light confinement effect, while under more standard condition the efficiency is around 1%, which is comparable to what we have achieved in this work.

* Corresponding author. Tel.: +39 011 670 7596; fax: +39 011 670 7591.
E-mail address: claudia.barolo@unito.it (C. Barolo).
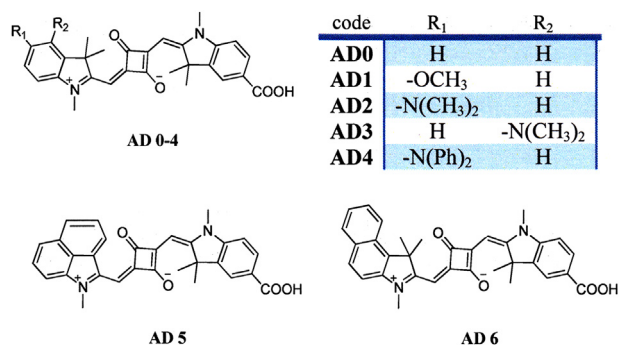[1] These authors contributed equally to this work.

Fig. 1. Molecular structures of the studied unsymmetrical squaraine dyes.

Squaraine dyes showing absorption maximum above 750 nm have been extensively studied as fluorescent probes [22–26], fluorochromes [27], photosensitizers in photodynamic therapy [28], fibre-optic sensors [29], as well as for their spectroscopic properties [30,31]. Recently, an unsymmetrical squaraine dimer synthesized through condensation on a symmetric bis-indolenine bridge, **BSQ01** (with $\lambda_{max} = 730$ nm in DMF), was used as sensitizer in DSCs, yielding 17% IPCE, and 1.3% cell efficiency (obtained under 100 mW cm^{-2} illumination intensity) [32]; squarylium dyes with similarly extended π conjugated systems, LSQa-c (having λ_{max} in the range between 777 and 800 nm in CHCl$_3$), showed conversion efficiencies up to 2.26% [33].

In the quest for new dyes having specific properties, it is important to be able to predict and select the characteristics for each proposed structure. We already successfully employed a computational approach to design and evaluate different cyanine dye structures before starting the synthesis process [34]. In the present work we evaluated several unsymmetrical squaraines bearing electron donating groups on one side of the molecule (Fig. 1) in terms of absorption range, in order to identify the most promising NIR absorbing dyes for in cell application. The selected structure, coded **AD5**, has been then synthesised and tested resulting in the **VG5** dye (see Scheme 1).

We recently reported a kinetic regeneration study for DSCs based on this novel unsymmetrical squaraine **VG5** which shed light on the mechanism and limits to the regeneration rate relative to oxidation potential [35]. Furthermore, measurements of the electron lifetime for a series of **VG5** based DSCs with varying free iodine concentration contributed to elucidate the mechanism of electron recombination to the electrolyte in DSCs based on the iodide/triiodide redox couple [13]. We note that in a recent work, a similar squaraine dye was published, called **SQ2**, which exhibits comparable spectroscopic, electrochemical and photovoltaic properties but with lower short circuit photocurrent and IPCE [36]

In this paper we report the results of the computational screening on various squaraine dyes and the synthesis, spectroscopic, electrochemical and photoelectrochemical characterization of this squaraine dye, **VG5**, which exhibits an atypical broad absorption band in the NIR region ranging from 600 to 850 nm. This squaraine was designed using 5-carboxy-2,3,3-trimethyl indolenine as an anchoring moiety, which showed promising efficiency results [37], and an *N*-alkylbenz[*cd*]indol-1-ium, known for extending absorption to the NIR region, due to its large π conjugation [38]

2. Experimental details

2.1. Computational analysis

The work was carried out within the Density Functional Theory (DFT) framework [39]. All dyes structures have been first fully optimized for the electronic ground state and then the optical properties have been calculated. The calculation of vertical excitation energy (VEE) and the oscillator strength of low-lying singlet excited state were carried out at the equilibrium geometry using Time Dependent DFT (TD-DFT) [40]. This method makes excited states calculations affordable for medium to large size molecules, but tends to overestimate transition energies; yet trends and comparison between parent molecules are very reliable. The screening over the entire set has been performed using the B3LYP exchange – correlation functional [41] and a standard 6-311G(d) triple zeta basis set. Further analysis on the better performing candidate, **VG5**, were carried on using the CAM-B3LYP functional [42], *i.e.* the B3LYP functional modified by Handy and coworkers using the Coulomb-attenuating method, to allow for the partial charge transfer nature of the electronic states of these type of molecules. All calculations have been performed using the Gaussian software [43].

2.2. Synthesis

Column chromatography was performed on Sigma Aldrich silica gel 60 (70–230 mesh ASTM). TLC was performed on Fluka silica gel TLC-PET foils GF 254, particle size 25 mm, medium pore diameter 60 A. Petroleum ether (PE) refers to the fraction boiling in the range 40–60 °C. ^{1}H NMR and ^{13}C NMR spectra were recorded on a Bruker Avance 200 spectrometer at 200 MHz and 50 MHz, respectively, in DMSO-d_6. Mass spectra were recorded on a Thermo Finnigan Advantage Max Ion Trap Spectrometer equipped with an electrospray ion source (ESI) in positive or negative ion acquiring mode. Commercially available reagents and solvents were purchased from Aldrich and used without further purification.
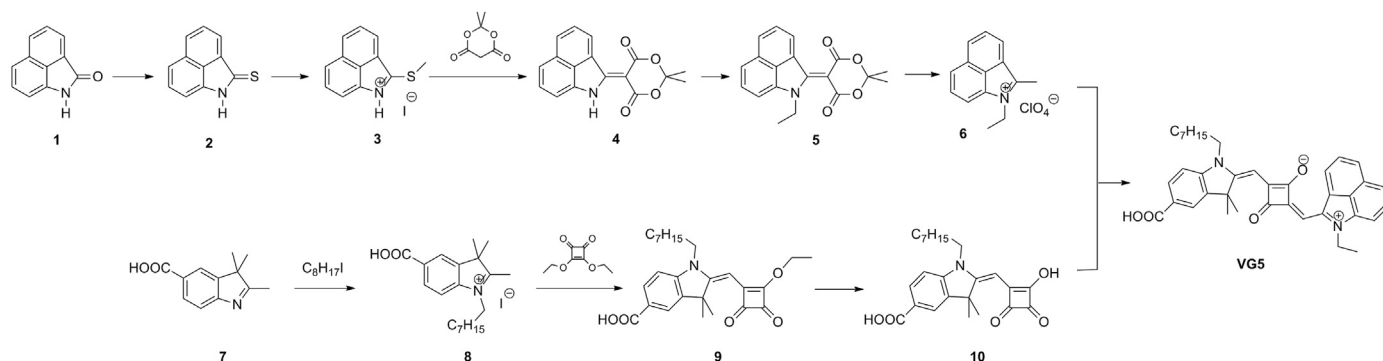
Scheme 1. Synthetic route to **VG5**.

Compounds **2**−**10** (Scheme 1) were synthesized by slightly modification of literature methods [5,32,44−47]. Detailed synthetic procedures and characterizations are available in the Supporting Information.

(E)-2-((E)-(5-carboxy-3,3-dimethyl-1-octylindolin-2-ylidene) methyl)-4-((1-ethylbenz[*cd*]indol-2-yl)methylene)-3-oxociclobut-1-enolate (VG5): 10 (0.200 g, 0.455 mmol) and 6 (0.135 g, 0.455 mmol) were heated under reflux in butanol/benzene (1:1, 40 mL) in a Dean−Stark apparatus for 3 h. Evaporation followed by flash chromatography ($CHCl_3/CH_3OH$ 9:1) yielded product 11 (0.027 g, yield = 10%). MS (ESI): m/z 587 $[M-1]^-$ ^{1}H NMR ($CDCl_3$): δ = 0.79 (t, J = 6.00 Hz, 3H, N−$(CH_2)_7$−CH_3), 1.18 (m, 12H, 6 CH_2), 1.37 (m, 3H, NCH_2CH_3), 1.78 (s, 6H, 2 CH_3), 3.99 (m, 2H, NCH_2), 4.16 (m, 2H, NCH_2), 6.04 (s, 1H, CH), 6.27 (s, 1H, CH), 6.96 (t, J = 6.00 Hz, 2H, H_{Ar}), 7.44 (m, 2H, H_{Ar}), 7.75 (t, J = 6.00 Hz, 2H, H_{Ar}), 7.86 (d, J = 4.00 Hz, 1H, H_{Ar}), 8.01 (m, 1H, H_{Ar}), 9.08 (m, 1H, H_{Ar}) ^{13}C NMR ($CDCl_3$): δ 13.60, 13.87, 19.09, 22.37, 26.79, 28.90, 29.12, 30.63, 31.51, 38.40, 43.79, 48.93, 88.66, 90.63, 106.60, 108.85, 121.44, 123.33, 125.32, 125.64, 128.18, 129.47, 130.23, 140.71, 142.04, 145.94, 151.24, 166.10, 170.10, 177.43, 182.7.

2.3. Spectroscopic characterization of **VG5**

UV−vis spectra were recorded on a Shimadzu UV-1700 spectrometer using different solvents in order to investigate the solvatochromic behaviour of **VG5**. A stock solution ($3.5 \cdot 10^{-3}$ M) in dimethyl sulfoxide (DMSO) was prepared and dilutions ($3.5 \cdot 10^{-5}$ M) in tetrahydrofuran (THF), dichloromethane (DCM), dimethyl sulfoxide (DMSO), acetonitrile (ACN), methanol and ethanol were analysed.

Fluorescence measurements were recorded using a Fluorolog 2 from Jobyn Ivon. The excitation wavelength was set at 710 nm. The range for fluorescence emission recording was from 735 to 1000 nm with slits at 14.7 nm.

2.4. Electrochemical characterization

Voltammetric measurements employed a PC controlled AutoLab PSTAT10 electrochemical workstation and were carried out in an Ar-filled glove box, oxygen and water <1 ppm. Cyclic Voltammetry and Differential Pulse Voltammetry techniques were used to estimate the redox potentials. CVs were obtained at a scan rate of 1 and 0.1 Vs^{-1}, DPVs were obtained at a Modulation Potential of 50 mV, a Step Potential of 10 mV, a Modulation Time of 50 ms and an Interval Time of 100 ms. Measurements were carried out using 0.1 M $TBAPF_6$ as supporting electrolyte in dimethylformamide (DMF). Glassy carbon, platinum plate and platinum wire were used as working, counter and quasi-reference electrodes, respectively. At the end of each measurement, ferrocene was added as internal reference. We have considered the redox couple Fc+/Fc to be located at 0.72 V vs NHE in DMF [48].

2.5. Cell preparation

TiO_2 (DSL18NRT) films were tape-cast onto transparent conductive F:SnO_2 (FTO) glass substrates, LOF Tec 15. They were heated to 450 °C in air for 30 min to give a layer thickness of 14 μm. After heating, a layer of Solaronix Ti300 paste was deposited on the film and heated at 450 °C in air for 30 min to give a 4 μm thick scattering layer. The standard $TiCl_4$ treatment was applied using a 30 mM $TiCl_4$ -tetrahydrofuran (THF) complex in water at 70 °C for 30 min [49]. After reheating to 450 °C for 30 min, the films were allowed to cool to ∼100 °C and then immersed in the dye solution for 3 h. The dye solution used was 0.26 mM **VG5** with 52 mM chenodeoxycholic acid (CDCA) in ethanol. CDCA concentration was

optimized to achieve an absorbance of 1. Counter electrodes were prepared by drilling two 0.8 mm holes through FTO glass before platinising them with H_2PtCl_6 (5 nM) in 2-propanol. Cells were sealed with 25 μm Surlyn gasket (Solaronix, Aubonne, Switzerland). Electrolyte was injected into the cells through the holes on the counter electrode. The electrolyte composition was 1 M Lithium perchlorate $LiClO_4$, 1 M 1-propyl-3-methyl imidazolium iodide (PMMI) and 40 mM I_2 in 3-methoxypropionitrile (MPN). Holes were sealed with a glass cover slip and Surlyn. The cell active area was 1 cm × 1 cm. Silver paint was applied onto the tin oxide on the four sides of the cells to reduce series resistance.

Transparent conductive F:SnO_2 (FTO) glass, LOF Tec 15, was purchased from Hartford Glass (Indiana, USA). TiO_2 nanoparticle paste DSL18NRT was purchased from DyeSol (NSW, Australia).

3. Results and discussion

3.1. Computational analysis

The design focused on the effect of substitutions on the optical properties of the dyes, in particular for the presence of electron donating groups. Unsymmetrical squaraine dyes carrying a −COOH group on one indolenine moiety and an electron rich group on the other have been studied (Fig. 1). The substituents used are: −OCH_3 moiety (**AD1**), −N$(CH_3)_2$ in R_1 (**AD2**) and R_2 (**AD3**) position, −NPh_2 (**AD4**) and fused benzene ring (**AD5** and **AD6**).

Results for the vertical excitation energy and the energy of the molecular orbitals involved in the main contributions are collected in Table 1. Only results for the most stable conformers are reported.

Among all dyes, AD5 (Fig. 2) is the one with the absorption maximum most shifted toward the near IR and has, therefore, been studied in more detail and later synthesised with the code **VG5**. The difference between model AD5 and the actual molecule **VG5** is in the alkylic substituents on the indolenine nitrogens, where both the C_8H_{17} chain and the ethyl group have been substituted with a methyl moiety. It is known that this kind of substitutions do not affect the results of the calculation, as the alkylic chains are not involved in the delocalized electron distribution, which is responsible for the optical properties of the dye. For this molecule, DFT predicts a planar dye skeleton, as expected for a large conjugated π system, and only small distortions are predicted on the aromatic substituents.

The Vertical Excitation Energies (VEE) have been calculated using the CAM-B3LYP functional for the first five lowest energy electronic transitions, and are reported in Table 2 together with the oscillator strength, and the description of the molecular orbitals involved in the corresponding transition.

The absorption spectra of AD5 (**VG5**) shows a strong, optically allowed, band at 606 nm, corresponding to the HOMO → LUMO transition, and a less intense band at 337 nm roughly corresponding to the HOMO → LUMO + 1 transition. As it can be noted from

Table 1
Calculated VEE, oscillator strength and dominant contributions of the main transition of the unsymmetrical dyes **AD1**−**AD6**.

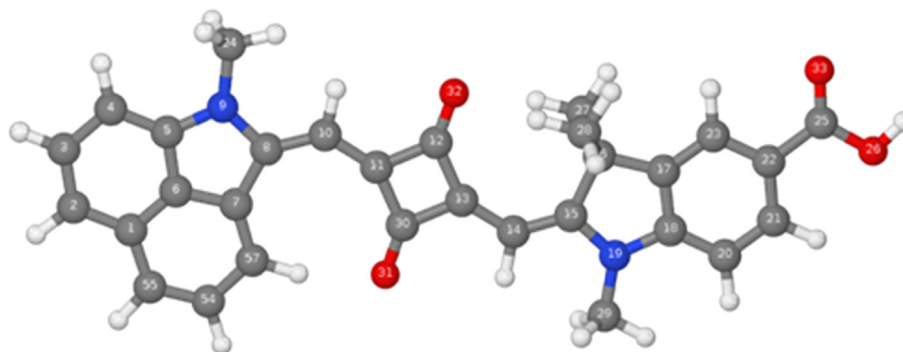| Dye	Irrep	VEE nm (eV)	Oscillator strength	Dominant contributions				
				occ. orb	E (eV)	virt. orb.	E (eV)	% contr.
AD1	a1	554 (2.24)	1.56	HOMO	−4.82	LUMO	−2.59	98
AD2	a1	572 (2.17)	1.58	HOMO	−4.66	LUMO	−2.48	97
AD3	a1	564 (2.20)	1.49	HOMO	−4.77	LUMO	−2.55	96
AD4	a1	623 (1.99)	0.54	HOMO-2	−5.87	LUMO	−3.00	69
	a2	622 (1.99)	1.36	HOMO	−5.00	LUMO	−3.00	69
AD5	A	656 (1.89)	1.30	HOMO	−4.88	LUMO	−3.04	98
AD6	a1	561 (2.21)	1.51	HOMO	−4.88	LUMO	−2.66	97

Fig. 2. Relaxed structure for **AD5**.

Table 2
Calculated VEE, oscillator strength and dominant contributions of the first five lowest energy electronic transitions of dye **AD5** (**VG5**).

Transition	VEE eV (nm)	Oscillator strength	Dominant contributions		
			occ. orb	virt. orb.	% contr.
1	606 (2.04)	1.43	HOMO	LUMO	98
2	456 (2.71)	0	HOMO-2	LUMO	92
3	349 (3.55)	0.01	HOMO-1	LUMO	72
4	337 (3.68)	0.12	HOMO	LUMO+1	84
5	331 (3.73)	0	HOMO-5	LUMO	92

Table 1 the other electronic transitions have a negligible oscillator strength. The molecular orbitals involved in the main adsorption transitions are shown in Fig. 3.

The strong discrepancy between the observed (about 770 nm, see Section 3.3) and the calculated absorption energies is a well documented problem of TD-DFT theory which tends to overestimate the electronic transitions energies for such systems, yet providing a qualitatively correct picture of the excitation process.

It can be noted that the HOMO → LUMO transition corresponds to a partial migration of the electronic charge from the squarainic ring to the benzoindolenine moiety. On the other hand, transitions involving the HOMO and the LUMO + 1 molecular orbitals are a clear-cut charge transfer transitions toward the carboxylic group.

Finally, it is worth noting that the model employed does not include Frank–Condon effects and cannot reproduce the other peaks experimentally observed which correspond to vibronic bands.

3.2. Synthesis of **VG5**

VG5 was synthesized by condensation of benzoindolenine salt **6** with emisquaraine **10**. **6** was prepared according to literature method from naphthostyryl **1**, via methylation of thionaphthostyryl **2** [44,45], protection with Meldrum's acid [46] followed by alkylation and deprotection [47]. A complete characterization of all the intermediates has been accomplished.

3.3. Photochemical and electrochemical properties of **VG5**

As reported in Fig. 4a, the Vis/NIR absorption spectrum of **VG5** in EtOH shows one shoulder and an absorption maximum at 722 nm and 768 nm, respectively. The solvatochromic shift of **VG5** was studied and is reported in Fig. 4b and Table 3. UV–vis absorption as well as steady-state fluorescence emission spectra show, in general, a negative solvatochromism which results from a higher polarity of the ground state with respect to the excited state [50,51]. The red-shift of 62 nm from **BSQ01** [32] absorption maximum at 730 nm in DMF is consistent with the expected effect of extending conjugation.
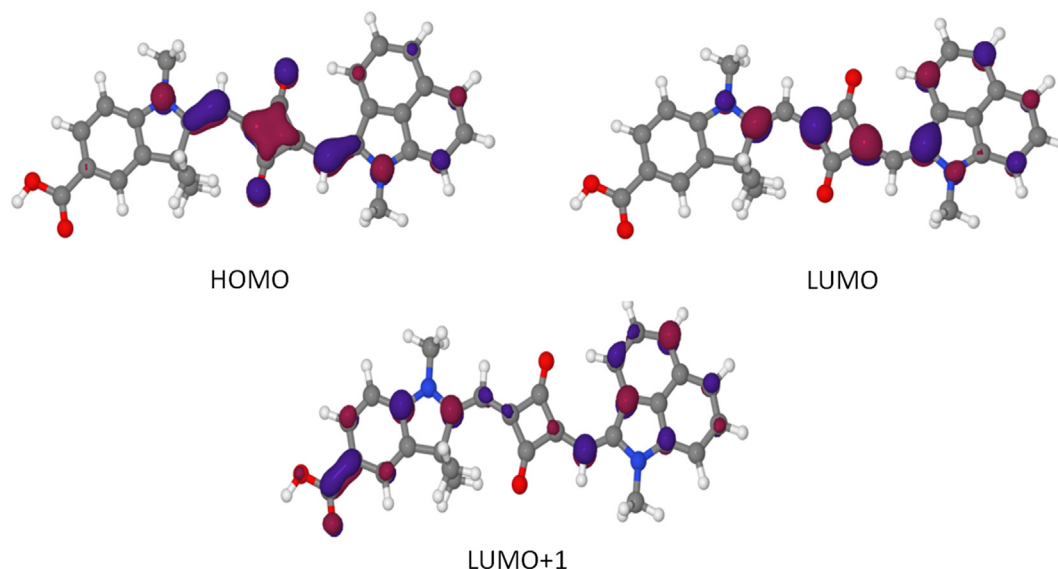

HOMO   LUMO

LUMO+1

Fig. 3. Representation of frontiers orbitals involved in adsorption spectra.
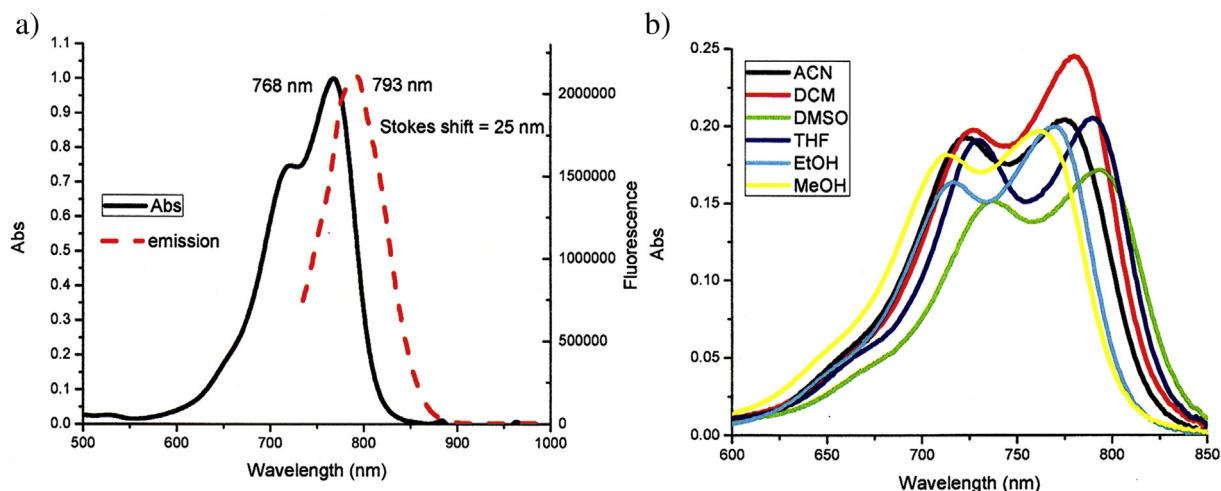
a)

b)

Fig. 4. a) Absorbance and fluorescence emission spectra in ethanol and b) solvatochromism of **VG5**.

Table 3
Spectroscopic properties of the solvatochromism of **VG5**.

	Shoulder λ_{max} [nm]	Main peak λ_{max} [nm]	λ_{em} [nm]	Stokes shift [nm]	E_{0-0}
THF	730	790	806	16	1.57
DCM	727	780	801	21	1.59
DMSO	737	792	813	21	1.57
ACN	723	775	800	25	1.60
EtOH	717	769	793	25	1.61
MeOH	713	762	783	21	1.63

The oxidation and reduction potentials of the dye are located respectively at +0.10 V and −1.16 V vs Fc+/Fc couple. The cyclic voltammogram shows quasi-reversible peaks (Fig. 5). Moreover, as can be observed from the DPV (dark blue curve, in web version), inducing a second reduction of the dye (−1.95 V vs Fc) gives rise to a decomposition product, which is oxidized at about −0.5 V vs Fc. The measured redox potential is used as an estimation of E^0. We assumed that the first oxidation potential (E^0_{ox}) and reduction potential (E^0_{red}) correspond to the HOMO and, with a larger approximation, to LUMO levels of the dye. Therefore, using the conversion

factor of Fc+/Fc 0.72 V vs NHE, the HOMO and LUMO levels are located at 0.82 and −0.44 V vs NHE for **VG5**. In the literature, the LUMO is also calculated by subtracting the value of the optical band gap E^{opt}_g from the value of the oxidation potential E^0_{ox}. This method provides the LUMO of the dye located at even lower levels. The value of the electrochemical potential of this dye is consistent for a possible fast regeneration while the injection can be affected from the fact that **VG5** LUMO is too low compared to the TiO$_2$ conduction band.

3.4. Cell performance

The cell I−V characteristics were measured using a 150W Xenon lamp filtered to simulate AM 1.5. The cell I−V plot for both 1 sun and dark short circuit current is shown in Fig. 6, as shown the short circuit maximum photocurrent (Jsc), the Open-Circuit voltage (Voc), the fill factor (FF) and the overall efficiency at AM 1.5 conditions were respectively 7.29 mA cm^{-2}, 0.35 V, 0.43 and 1.10%. The low voltage for this cell is due to the very high Lithium content of the electrolyte (1 M), and the absence of base. This composition was required to lower the TiO$_2$ conduction band edge to allow injection

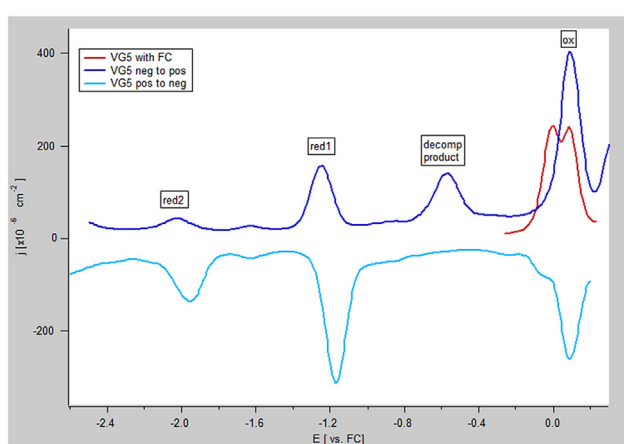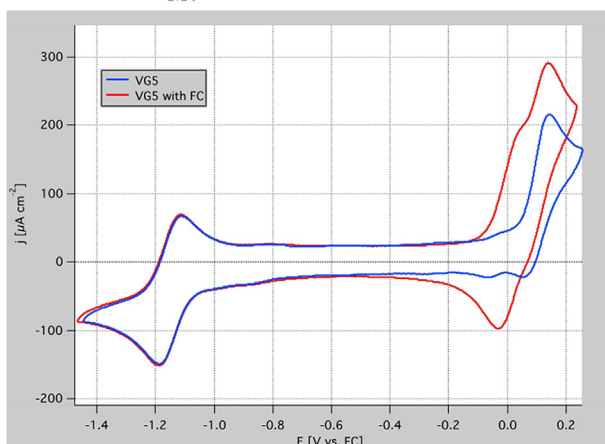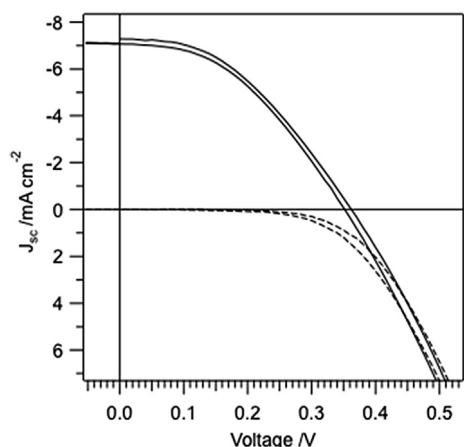|	E1 (ox)	E2 (red)
VG5	0.10	−1.16

Fig. 5. CVs of **VG5**, before (blue) and after Fc addition, scan rate 100 mVs^{-1} (left) and DPV in a large V-range of **VG5**, red curve obtained after Fc addition (right). (For interpretation of the references to colour in this figure legend, the reader is referred to the web version of this article.)

Fig. 6. Comparison of the cyclic I—V measurements for a **VG5** DSC cell in the dark (dashed line) and under 100 mW/cm^2 (A.M.1.5G) light illumination (solid line). Measures are done cyclically and two lines are reported for each type of measure. Cell construction as given in the experimental.

from the low lying LUMO of this dye. The LUMO lies at -0.44 V vs NHE, 0.26 V below the conduction band edge in standard solvents (-0.7 V vs NHE). The voltage loss with respect to the standard cells with N719 dye (~ 0.75 V) reflects mainly the change in electrolyte, though there may also be a contribution from enhanced recombination.

IPCE measurements were performed using a shuttered monochromated light source where the intensity was calibrated using a UV-enhanced silicon photodiode. Incident photon conversion efficiency is plotted against the absorption spectrum of **VG5**. The implied "1 sun" photocurrent calculated by integrating the IPCE with the AM 1.5 spectral intensity, is 6.7 mA cm^{-2}, which is quite close to the 7 mA cm^{-2} measured. The dye shows a maximum quantum efficiency of 36% at 800 nm. As virtually all light was absorbed at this wavelength, this also corresponds to an absorbed photon to current efficiency (APCE) of 36%. Interestingly, the APCE at wavelengths below 624 appears to be larger, even allowing for increased absorption in the cell due to the scattering layer. This result is in line with the calculated DFT data, for example the enhanced APCE at 440 nm can be explained by the participation in
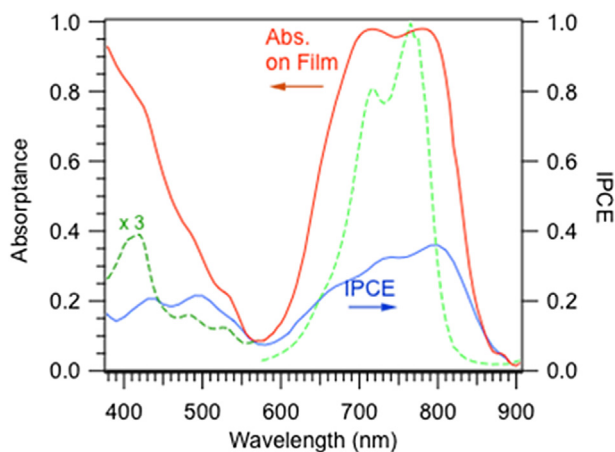
the transition of the HOMO $-$ 2 and LUMO $+$ 1 molecular orbitals; as noted above, this transition involves a D$-\pi-$A charge transfer across the molecule which gives the correct directionality for electron injection. The absorption spectrum of the dye solution is included for comparison (Fig. 7). In the IPCE spectrum, some peaks have clearly shifted, most likely due to the change in solvent and solvatochromism of the dye.

4. Conclusions

The design, synthesis and characterization, as well as the full characterization of all the intermediates, of a near infrared dye, coded **VG5**, was accomplished. This dye was selected among a variety of candidates as NIR absorbing dyes: the screening was performed using a computational approach, thus evaluating the optical properties of a range of promising dye structures using a TD-DFT approach prior the synthetic steps. The selected dye was then spectroscopically and electrochemically characterized showing a negative solvatocromism and a presumed fast regeneration but a low LUMO level. DSCs based on TiO$_2$ photoelectrodes dyed with **VG5** were fabricated and the photovoltaic properties were characterized under AM 1.5 irradiation. An overall energy efficiency of 1.1% and IPCE of 36% at 800 nm were achieved with a standard TiO2 layer. This result shed light to possible future NIR structures to be used as sensitizers for DSCs. Actually, even if **VG5** has shown a limited efficiency, its strong absorption at 780 nm makes it a useful system for fundamental mechanistic studies on NIR dyes [13,35].

Appendix A. Supplementary data

Supplementary data related to this article can be found at http://dx.doi.org/10.1016/j.renene.2013.06.018.

Fig. 7. Absorbance (1-T) and IPCE (spectral response) of **VG5**. Absorbance is from a dyed TiO$_2$ plate without scattering layer. Absorption of dye in solution is also included for comparison (green dotted, arbitrary units), and it is amplified in the region 380—580 nm. (For interpretation of the references to colour in this figure legend, the reader is referred to the web version of this article.)

References

[1] O'Regan B, Grätzel M. A low-cost, high-efficiency solar cell based on dye-sensitized colloidal TiO$_2$ films. Nature 1991;353:737—40.
[2] Yella A, Lee H-W, Nok Tsao H, Yi C, Chandiran AK, Nazeeruddin MdK, et al. Porphyrin-sensitized solar cells with cobalt (II/III)—based redox electrolyte exceed 12 percent efficiency. Science 2011;334:629—34.
[3] (a) Nazeeruddin Md K, De Angelis F, Fantacci S, Selloni A, Viscardi G, Liska P, et al. Combined experimental and DFT-TDDFT computational study of photoelectrochemical cell ruthenium sensitizers. J Am Chem Soc 2005;127: 16835—47;
(b) Sauvage F, Decoppet JD, Zhang M, Zakeeruddin SM, Comte P, Nazeeruddin Md K, et al. Effect of sensitizer adsorption temperature on the performance of dye-sensitized solar cells. J Am Chem Soc 2011;133:9304—10;
(c) Gao F, Wang Y, Shi D, Zhang J, Wang M, Jing X, et al. Enhance the optical absorptivity of nanocrystalline TiO$_2$ film with high molar extinction coefficient ruthenium sensitizers for high performance dye-sensitized solar cells. J Am Chem Soc 2008;130:10720—8.
[4] (a) Park J, Viscardi G, Barolo C, Barbero N. Near-infrared sensitization in dye-sensitized solar cells. Chimia 2013;67:129—35;
(b) Yum J-H, Baranoff E, Wenger S, Nazeeruddin Md K, Grätzel M. Panchromatic engineering for dye-sensitized solar cells. Energy Environ Sci 2011;4: 842—57.

[5] Yum J-H, Walter P, Huber S, Rentsch D, Geiger T, Nüesch F, et al. Efficient far red sensitization of nanocrystalline TiO_2 films by an unsymmetrical squaraine dye. J Am Chem Soc 2007;129:10320–1.

[6] Mori S, Nagata M, Nakahata Y, Yasuta K, Goto R, Kimura M, et al. Enhancement of incident photon-to-current conversion efficiency for phthalocyanine-sensitized solar cells by 3D molecular structuralization. J Am Chem Soc 2010;132:4054–5.

[7] Jiao C, Zu N, Huang K-W, Wang P, Wu J. Perylene anhydride fused porphyrins as near-infrared sensitizers for dye-sensitized solar cells. Org Lett 2011;13:3652–5.

[8] Takechi K, Kamat PV, Avirah RR, Jyothish K, Ramaiah D. Harvesting infrared photons with croconate dyes. Chem Mater 2008;20:265–72.

[9] Mishra A, Fischer MKR, Bäuerle P. Metal-free organic dyes for dye-sensitized solar cells: from structure: property relationship to design rules. Angew Chem Int Ed 2009;48:2474–99.

[10] Ooyama Y, Harima Y. Molecular designs and syntheses of organic dyes for dye-sensitized solar cells. Eur J Org Chem 2009:2903–34.

[11] a) Luo S, Zhang E, Su Y, Cheng Tn, Shi C. A review of NIR dyes in cancer targeting and imaging. Biomaterials 2011;32:7127–38;
b) Avirah RR, Jayaram DT, Adarsh N, Ramaiah D. Squaraine dyes in PDT: from basic design to in vivo demonstration. Org Biomol Chem 2012;10:911–20.

[12] Beverina L, Salice P. Squaraine compounds: tailored design and synthesis towards a variety of material science applications. Eur J Org Chem 2010:1207–25.

[13] Richards CE, Anderson AY, Martiniani S, Law C, O'Regan BC. The mechanism of iodine reduction by TiO_2 electrons and the kinetics of recombination in dye-sensitized solar cells. J Phys Chem Lett 2012;3:1980–4.

[14] Paek S, Choi H, Kim C, Cho N, So S, Song K, et al. Efficient and stable panchromatic squaraine dyes for dye-sensitized solar cells. Chem Commun 2011;47:2874–6.

[15] Barolo C, Yum J, Artuso E, Barbero N, Di Censo D, Lobello MG, et al. A simple synthetic route to obtain pure trans-ruthenium(II) complexes for dye sensitized solar cell applications. Chem Sus Chem 2013. http://dx.doi.org/10.1002/cssc.201200973.

[16] Abbotto A, Sauvage F, Barolo C, De Angelis F, Fantacci S, Grätzel M, et al. Panchromatic ruthenium sensitizer based on electron-rich heteroarylvinylene π-conjugated quaterpyridine for dye-sensitized solar cells. Dalton Trans 2011;40:234–42.

[17] Barolo C, Nazeeruddin Md K, Fantacci S, Di Censo D, Comte P, Liska P, et al. Synthesis, characterization, and DFT-TDDFT computational study of a ruthenium complex containing a functionalized tetradentate ligand. Inorg Chem 2006;45:4642–53.

[18] Nazeeruddin MK, Péchy P, Renouard T, Zakeeruddin SM, Humphry-Baker R, Comte P, et al. Engineering of efficient panchromatic sensitizers for nanocrystalline TiO_2-based solar cells. J Am Chem Soc 2001;123:1613–24.

[19] Miao Q, Gao J, Wang Z, Yu H, Luo Yi, Ma T. Syntheses and characterization of several nickel bis(dithiolene) complexes with strong and broad near-IR absorption. Inorg Chim Acta 2011;376:619–27.

[20] Saji VS, Zong K, Pyo M. NIR absorbing poly(thieno[3,4b]thiophene2carboxylic acid) as a polymer dye for dyesensitized solar cells. J Photochem Photobiol A: Chem 2010;212:81–7.

[21] Ono T, Yamaguchi T, Arakawa H. Study on dye-sensitized solar cell using novel infrared dye. Sol Energy Mater Sol Cells 2009;93:831–5.

[22] Eldo J, Ajayaghosh A. New low band gap polymers: control of optical and electronic properties in near infrared absorbing π-conjugated polysquaraines. Chem Mater 2002;14:410–8.

[23] Sreejith S, Divya KP, Ajayaghosh A. A near-infrared squaraine dye as a latent ratiometric fluorophore for the detection of aminothiol content in blood plasma. Angew Chem Int Ed 2008;47:7883–7.

[24] Umezawa K, Citterio D, Suzuki K. Water-soluble NIR fluorescent probes based on squaraine and their application for protein labeling. Anal Sci 2008;24:213–7.

[25] Basheer MC, Santhosh U, Alex S, Thomas KG, Suresh CH, Das S. Design and synthesis of squaraine based near infrared fluorescent probes. Tetrahedron 2007;63:1617–23.

[26] Patsenker L, Tatarets A, Kosolova O, Obukhova O, Povrozin Y, Fedyunyayeva I, et al. fluorescent probes and labels for biomedical applications. Ann N.Y Acad Sci 2008;1130:179–87.

[27] Pham W, Weissleder R, Tung C-H. An azulene dimer as a near-infrared quencher. Angew Chem Int Ed 2002;41:3659–62.

[28] Beverina L, Crippa M, Landenna M, Ruffo R, Salice P, Silvestri F, et al. Assessment of water-soluble π-extended squaraines as one and two-photon singlet oxygen photosensitizers: design, synthesis, and characterization. J Am Chem Soc 2008;130:1894–902.

[29] Šimon P, Sekretár S, MacCraith BD, Kvasnik F. Near-infrared reagents for fibre-optic ammonia sensors. Sens Actuator B-chem 1997;39:252–5.

[30] Meier H, Petermann R. NIR absorbing squaraines by extension of the conjugation with (aminothiazolyl)ethenyl groups. Helv Chim Acta 2004;87:1109–18.

[31] Yagi S, Nakasaku Y, Maeda T, Nakazumi H, Sakurai Y. Synthesis and near-infrared absorption properties of linearly π-extended squarylium oligomers. Dyes Pigment 2011;90:211–8.

[32] Kuster S, Sauvage F, Nazeeruddin Md K, Grätzel M, Nüesch FA, Geiger T. Unsymmetrical squaraine dimer with an extended π-electron framework: an approach in harvesting near infra-red photons for energy conversion. Dyes Pigment 2010;87:30–8.

[33] Maeda T, Hamamura Y, Miyanaga K, Shima N, Yagi S, Nakazumi H. Near-infrared absorbing squarylium dyes with linearly extended π-conjugated structure for dye-sensitized solar cell applications. Org Lett 2011;13:5994–7.

[34] Benzi C, Bertolino CA, Miletto I, Ponzio P, Barolo C, Viscardi G, et al. The design, synthesis and characterization of a novel acceptor for real time polymerase chain reaction using both computational and experimental approaches. Dyes Pigment 2009;83:111–20.

[35] Martiniani S, Anderson AY, Law C, O'Regan BC, Barolo C. New insight into the regeneration kinetics of organic dye sensitised solar Cells. Chem Commun 2012;48:2406–8.

[36] Maeda T, Shima N, Tsukamoto T, Yagi S, Nakazumi H. Unsymmetrical squarylium dyes with π-extended heterocyclic components and their application to organic dye-sensitized solar cells. Synth Met 2011;161:2481–7.

[37] Park J, Barolo C, Sauvage F, Barbero N, Benzi C, Quagliotto P, et al. Symmetric vs asymmetric squaraines as photosensitisers in mesoscopic injection solar cells: a structure-property relationship study. Chem Commun 2012;48:2782–4.

[38] Yagi S, Hyodo Y, Matsumoto S, Takahashi N, Kono H, Nakazumi H. Synthesis of novel unsymmetrical squarylium dyes absorbing in the near-infrared region. J Chem Soc Perkin Trans 2000;1:599–603.

[39] Dreizler R, Gross E. Density functional theory. New York: Plenum Press; 1995.

[40] a) Bauernshmitt R, Ahlrichs R. Treatment of electronic excitations within the adiabatic approximation of time dependent density functional theory. Chem Phys Lett 1996;256:454–64;
b) Stratmann RE, Scuseria GE, Frisch MJ. An efficient implementation of time dependent density-functional theory for the calculation of excitation energies of large molecules. J Chem Phys 1998;109:8218–24.

[41] Becke AD. Density-functional thermochemistry. III. The role of exact exchange. J Chem Phys 1993;98:5648–52.

[42] Yanai T, Tew D, Handy N. A new hybrid exchange-correlation functional using the Coulomb-attenuating method (CAM-B3LYP). Chem Phys Lett 2004;393:51–7.

[43] Frisch MJ, Trucks GW, Schlegel HB, Scuseria GE, Robb MA, Cheeseman JR, et al. Gaussian 09. Wallingford CT: Gaussian, Inc.; 2009.

[44] Ficken GE, Kendall JD. The reactivity of the alkylthio-group in nitrogen ring compounds. Part III. 2-Methylthiobenz[cd]indole and its methiodide. J Chem Soc 1960;1537–41.

[45] Lakshmikantham MV, Chen W, Cava MP. Thioanhydrides. 3. Synthesis, properties and Diels-Alder reactions of sulfur analogs of 1,8-naphthalic anhydride. J Org Chem 1989;54:4746–50.

[46] Vasilenko NP, Mikhailenko FA, Rozhinsky JI. 2-Methylbenz[c, d]indole and its derivatives. Dyes Pigment 1981;2:231–7.

[47] Yagi S, Maeda K, Nakazumi H. Photochromic properties of cationic merocyanine dyes. thermal stability of the spiropyran form produced by irradiation with visible light. J Mater Chem 1999;9:2991–7.

[48] Zoski Cynthia G, editor. Handbook of electrochemistry. Elsevier; 2006.

[49] O'Regan BC, Durrant JR, Sommeling PM, Bakker NJ. Influence of the TiCl4 treatment on nanocrystalline TiO_2 films in dye-sensitized solar cells. 2. Charge density, band edge shifts, and Quantification of recombination Losses at short circuit. J Phys Chem C 2007;111:14001–10.

[50] Tatikolov AS, Costa SMB. Photophysical and aggregation properties of a long-chain squarylium indocyanine dye. J Photochem Photobiol A 2001;140:147–56.

[51] Gude C, Rettig W. Radiative and nonradiative excited state relaxation channels in squaric acid derivatives bearing differently sized donor substituents: a comparison of experiment and theory. J Phys Chem A 2000;104:8050–7.